JTTEES 4:179-184

High-Velocity Oxyfuel Thermal Spray Coatings for Biomedical Applications

J.D. Haman, A.A. Boulware, L.C. Lucas, and D.E. Crawmer

Plasma spraying is used to produce most commercially available bioceramic coatings for dental implants; however, these coatings still contain some inadequacies. Two types of coatings produced by the high-velocity oxyfuel (HVOF) combustion spray process using commercially available hydroxyapatite (HA) and fluorapatite (FA) powders sprayed onto titanium were characterized to determine whether this relatively new coating process can be applied to bioceramic coatings. Diffuse reflectance Fourier transform infrared (FTIR) spectroscopy, x-ray diffraction (XRD), and scanning electron microscopy (SEM) were used to characterize the composition, microstructure, and morphology of the coatings. The XRD and FTIR techniques revealed an apatitic structure for both HA and FA coatings. However, XRD patterns indicated some loss in crystallinity of the coatings due to the spraying process. Results from FTIR showed a loss in the intensity of the OH^- and F^- groups due to HVOF spraying; the phosphate groups, however, were still present. Analysis by SEM showed a coating morphology similar to that obtained with plasma spraying, with complete coverage of the titanium substrate. Interfacial SEM studies revealed an excellent coating-to-substrate apposition. These results indicate that with further optimization the HVOF thermal spray process may offer another method for producing bioceramic coatings.

1. Introduction

A MAJOR need for orthopedic and dental implants is improvement of long-term implant stabilization. Many methods of stabilization have been attempted, often with mixed results. The use of ceramic coatings on press-fit metallic implants is one area of study. These ceramic coatings have the same chemistry and structure as the mineral component of bone (Ref 1). The purpose of the implant coatings is to bond with the adjacent osseous tissue. The application of ceramic coatings can be achieved in several ways, such as ion beam sputter deposition, electrophoretic deposition, and plasma spraying (Ref 1-6). However, these methods of coating often induce material transformations due to excessive heating at some point in the coating process (Ref 7-9). Other problems such as poor coating-to-substrate bond strength and the presence of cracking and porosity have been noted (Ref 10, 11).

Ceramics such as hydroxyapatite (HA) and fluorapatite (FA) at elevated temperatures (beginning around 1300 °C) initially transform into α-tricalcium phosphate and upon further heating transform to tetracalcium phosphate and calcium oxide. These materials have mechanical properties and solubilities different from those of HA and FA (Ref 12-14). In most dental applications, the solubility and mechanical properties of these bioceramic coatings are of great importance—especially the effect of these properties on implant stabilization.

Other factors that affect implant stabilization include coating crystallinity and density. The typical plasma spray process heats the sprayed materials to melting. In bioceramics, although this increases adhesion of the coating material to the substrate, it also increases the amount of phase transformations and the amorphous content of the coatings. This increase in amorphous content increases the solubility of the coatings and may decrease the effectiveness of the implant. A less dense coating will also reduce that effectiveness by reducing the mechanical strength and increasing the solubility of the coating (Ref 15-17).

The present study has employed high-velocity oxyfuel (HVOF) thermal spraying to produce HA or FA coatings on titanium. The starting powders and as-sprayed coatings were analyzed chemically, microstructurally, and morphologically.

Keywords: biomedical coatings, Fourier transform infrared spectroscopy, HVOF, hydroxyapatite, phase structure

J.D. Haman, A.A. Boulware, and **L.C. Lucas,** University of Alabama at Birmingham, Department of Biomedical Engineering, Birmingham, AL 35294, USA; **D.E. Crawmer,** Miller Thermal, Inc., Appleton, WI 54912, USA

2. Materials

Hydroxyapatite and fluorapatite powders were obtained from Miller Thermal, Inc. (Appleton, WI). The diameter of the HA powders ranged from 15 to 118 μm (a mean size of 37.6 ± 0.394 μm was determined by sieving), while the FA particles ranged from 22 to 79 μm (Fig. 1), with a mean size of 40.12 ± 0.4153 μm. Rectangular titanium (ASTM F 67) coupons were obtained from Metal Samples, Inc. (Munford, AL). The coupons were ultrasonically cleaned, sandblasted with 60 grit Al_2O_3 at 40 psi, rinsed in alcohol to remove any remaining contaminants, and then coated with either HA or FA.

3. Methods

In this study, HVOF spraying was performed using hydrogen as the primary fuel and nitrogen as the carrier gas. Spraying parameters are shown in Table 1.

Chemical analysis of the powders and as-sprayed coatings was performed using a Mattson Research Series Fourier transform infrared (FTIR) (Mattson Research Series FTIR, ATI Instruments, North America, New Hope, PA) spectrometer with a Spectra-Tech (Spectra-Tech, Inc., Stamford, CT) diffuse reflec-

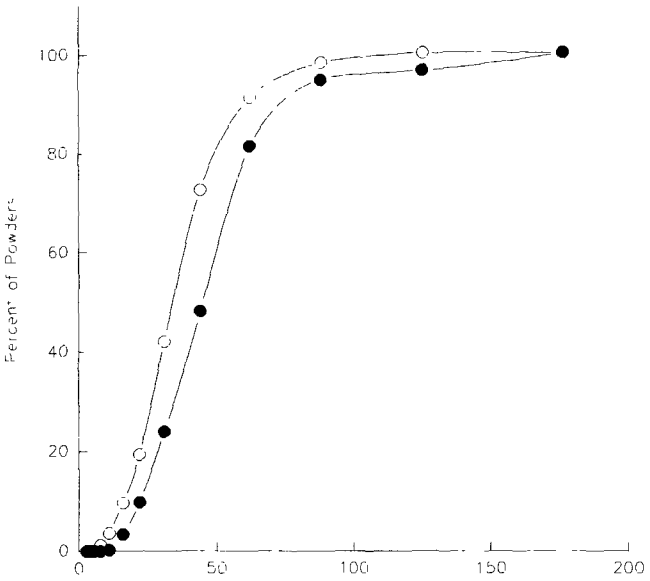

Fig. 1 Powder particle size distribution for both HA (o) and FA (●)

Table 1 HVOF spraying parameters

Parameter	HA coating	FA coating
Gun type	HV 2000	HV 2000
Nozzle size, mm	19	19
Spray distance, mm	304.8	304.8
Traverse speed of gun, m/min	30.48	30.38
Increment, mm	2.54	2.54
Preheat substrate	No	No
Oxygen (at 1.03 MPa), L/min	235.96	235.96
Fuel (H_2) (at 1.03 MPa), L/min	566.30	566.30
Carrier (N2) (at 0.69 MPa), L/min	16.52	16.52
Powder, g/min	15	15

tance accessory. For these analyses, both the starting powders and powders scraped from the as-sprayed coatings were mixed with potassium bromide (KBr) in a 1:99 ratio. Mid-range (from 4000 to 500 cm^{-1}) FTIR spectra were taken with the use of a liquid-nitrogen-cooled detector. The resulting spectra were then plotted with the wavenumbers (cm^{-1}) versus Kubelka-Munk units. Kubelka-Munk units are the result of a normalizing program that removes spectral reflectance from the spectrum. Triplicate samples of the starting powders and as-sprayed coatings were analyzed.

Structural analysis of the powders and as-sprayed coatings was conducted using a Siemens D500 (Siemens Analytical X-ray Instruments, Inc., Madison, WI, USA) diffractometer at 40 keV and 30 mA. Scans were run from 10° to 60° 2θ with a step of 0.02 and a time increment of 3 s. Copper K_α x-rays, of wavelength 1.5418 Å, were generated and incident x-rays passed through 1°, 0.6°, and 0.05° slits of the x-ray diffractometer (XRD). Triplicate samples of each starting powder and as-sprayed coating were analyzed. Crystalline structure (lattice parameters) and interplanar spacings were determined to compare the starting powders and as-sprayed coatings to JCPDS (Joint Committee on Powder Diffraction Standards) standards for HA and FA.

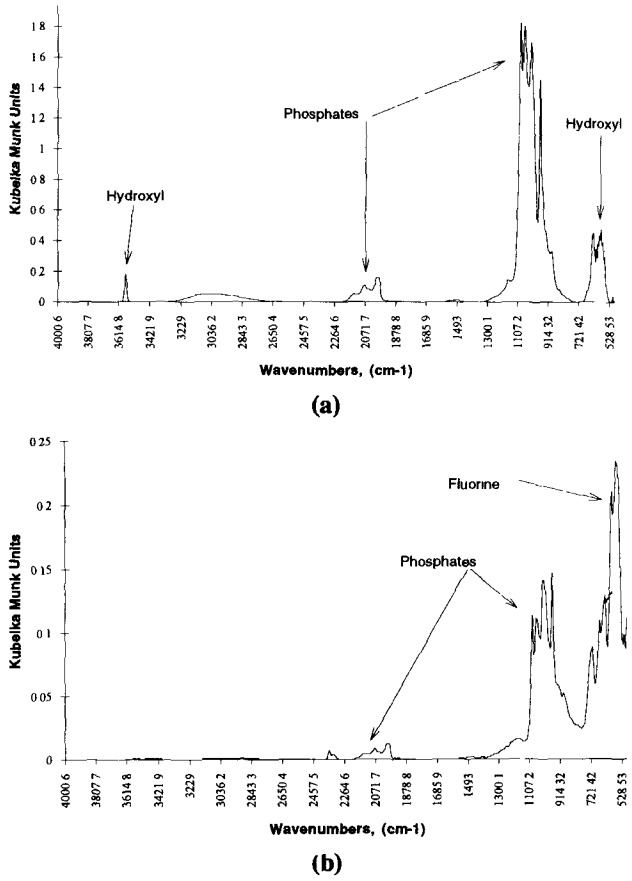

Fig. 2 FTIR of starting powders. (a) HA. (b) FA

Morphology was analyzed using a Philips 515 (Philips Electronics North America, New York, NY, USA) scanning electron microscope (SEM). Three topographical samples and three cross sections from each coating were studied. All samples were coated with approximately 20 nm Au-Pd to prevent charging. Interfacial samples were ground and polished using 60 through 1500 grit SiC paper and 1.0 through 0.05 μm Al_2O_3 slurries.

4. Results

Analyses of the HA and FA starting powders by FTIR and XRD revealed an apatitic structure. The presence of hydroxyl (3570 cm^{-1}) and fluor (630 cm^{-1}) groups in the HA and FA powders, respectively (Fig. 2), was indicated by FTIR analysis. Phosphate groups characteristic of the apatitic structure of HA and FA are noted in Fig. 2(a) and (b). Some carbonates (broad band around 1450 cm^{-1}) were found in both powders. X-ray diffraction analysis (Fig. 3) indicated that the powders matched JCPDS files for HA (9-0432) and FA (15-0876) in both peak positions and lattice parameters. These powders were highly crys-

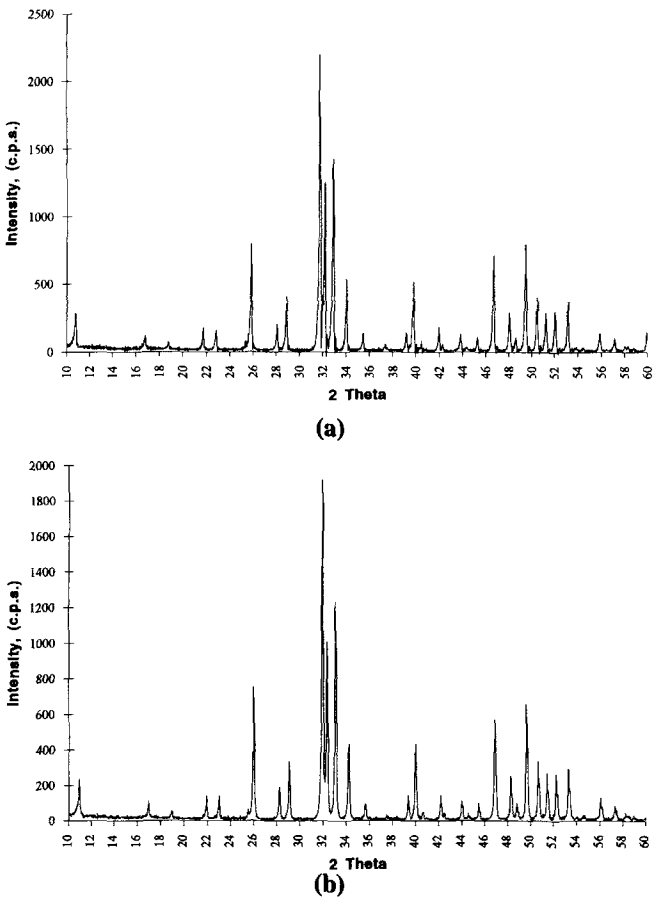

Fig. 3 XRD of starting powders. (a) HA. (b) FA

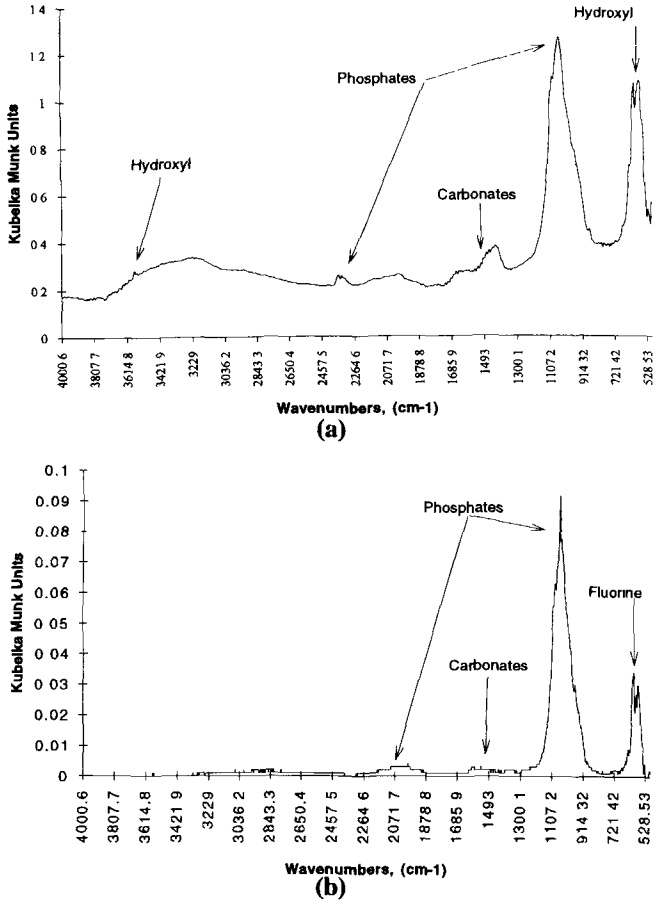

Fig. 4 FTIR of as-sprayed coatings. (a) HA. (b) FA

Table 2 Lattice parameters for the apatite materials

Material	HA (Å)	FA (Å)
JCPDS	$a = 9.418$	$a = 9.382$
	$c = 6.884$	$c = 6.880$
Starting powder	$a = 9.491 \pm 0.009$	$a = 9.3427 \pm 0.015$
	$c = 6.912 \pm 0.013$	$c = 6.8575 \pm 0.013$
As-sprayed coating	$a = 9.41 \pm 0.005$	$a = 9.3715 \pm 0.007$
	$c = 6.88 \pm 0.011$	$c = 6.8574 \pm 0.007$

talline, as can be seen by the sharp peaks and flat baselines in Fig. 3. Lattice parameter data are given in Table 2. Both the HA and FA starting powders had very similar lattice parameters compared to those found in JCPDS card files for the respective materials. However, since JCPDS does not include standard deviation information, it cannot be determined whether a for both powders is significantly different from the standards. Lattice parameters a and c appear to be slightly higher for the HA powders and lower for the FA powders.

Analyses by FTIR and XRD of the as-sprayed HA and FA coatings also revealed an apatitic structure. The FTIR spectra of the as-sprayed coatings indicated that some hydroxyl and fluor groups were lost, which is seen as a relative loss in peak intensity (Fig. 4). The phosphate peaks lost definition and merged into a broad single peak centered around 1060 cm^{-1} in the FA coatings and 1050 cm^{-1} in the HA coatings. Although no significant peaks for other phases were seen, small shoulders, possibly indicating phases such as β-TCP (875 cm^{-1}), were observed. Carbonate peaks (1400 cm^{-1}) were also noted in both coating materials.

Overall XRD patterns showed that the coatings matched peak positions and lattice parameters with those of JCPDS files for HA and FA, respectively. As-sprayed coating XRD results (Fig. 5) show that the baselines for both HA and FA are no longer flat, with bulges centered around 30° and 49° 2θ, and indicate that crystallinity has been reduced. Lattice parameter data are given in Table 2. Student's t-tests of the lattice parameters showed no significant difference ($\alpha = 0.05$) between the starting powder lattice parameters and the as-sprayed coating lattice parameters.

Topographical micrographs of the as-sprayed coatings (Fig. 6) show coatings composed of splats, granular areas, and respheroidized droplets. The coatings were contiguous, with any cracking confined within the splats. Interfacial or cross-sectional micrographs (Fig. 7) exhibit no cracking within the bulk of the coatings; however, porosity on a very small scale was observed. This porosity was partly due to the polishing process. Close apposition of the coating to the substrate was noted for both HA and FA as-sprayed coatings. The interfacial micrographs also indicate a lamellar coating structure.

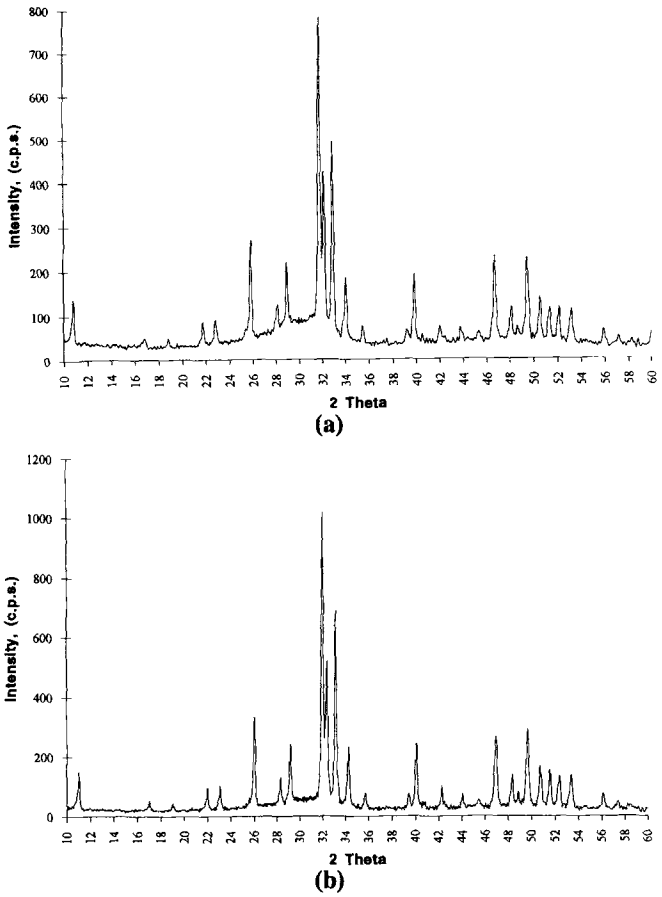

Fig. 5 XRD of as-sprayed coatings. (a) HA. (b) FA

5. Discussion

Comparison of the as-sprayed FTIR spectra for the HA and FA coatings with the spectra for their respective starting powders reveals a loss of intensity and definition of the hydroxyl, fluor, and phosphate peaks. Coupled with the loss of peak intensity and baseline flatness observed in the XRD spectra of the as-sprayed powders, this indicates a decrease in crystallinity as compared to the starting powders. This loss of crystallinity is most probably due to the partial to complete loss of long-range atomic order, or "melting," of the mid-range and smaller particles in the starting powder during the coating application. The presence of secondary phases is also evident in FTIR and XRD spectra of both coatings. However, the relatively sharp peaks with no significant shifts (seen in both FTIR and XRD spectra of the coatings) suggests that the "molten" particles were a very small component of the coatings. Again, the melting of some particles indicates that processing temperatures were sufficiently high to cause at least some phase transformations. Results of both FTIR and XRD analyses show some peak broadening and loss of symmetry; however, the XRD results suggest that the extra phases were a very small component of the coatings. The lattice parameter data for the HA and FA starting powders were very similar to those of the JCPDS standards; some differences in the *a* parameter may be due to the influence of the carbonates observed in the FTIR analyses (Ref 11). The

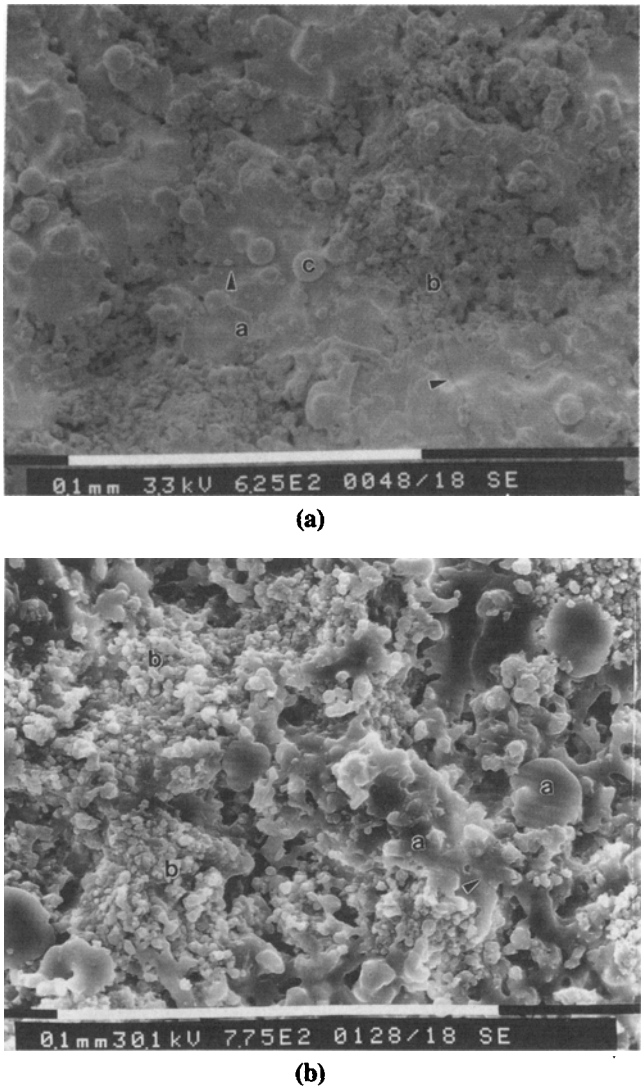

Fig. 6 Topographical SEMs of as-sprayed coatings. Arrows indicate cracking within the splats. Splats, granular areas, and resolidified droplets are indicated by a, b, and c, respectively. (a) HA. (b) FA

lattice parameters of the coatings were not significantly different from the starting powders, indicating that some other phases may still be present. Carbonates and other phases were also observed in the FTIR analyses of the as-sprayed coatings.

As with plasma spraying, the topography of coatings created by HVOF thermal spraying is dependent, in part, on the size of the starting powders. Powder sizes from 15 to 30 μm tend to lose long-range order and respheroidize, whereas larger particles (80 to 120 μm) tend to result in granular areas. Splats are usually formed by the mid-range particles (i.e., 50 to 80 μm) (Ref 18). The topography of the FA coatings indicates that the particle sizes present in the starting powder were primarily mid to high range. This agrees with the actual size range of the starting powders. The HA topography also agrees with the wide range (15 to 118 μm) of the starting powders, containing all three types of morphology.

The lamellar structure visible in the cross-sectional micrographs is due to the layering of splats, granular areas, and re-

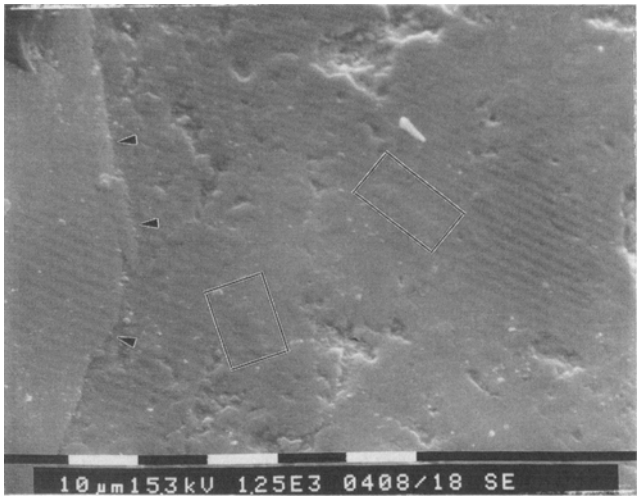

(a)

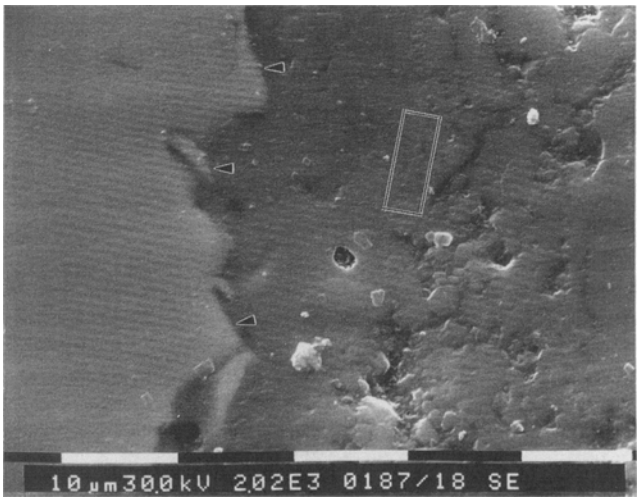

(b)

Fig. 7 Cross-sectional SEMs of as-sprayed coatings. The coating/substrate interface is indicated by arrows. Areas of apparent lamellar structure are circled. (a) HA. (b) FA

spheroidized droplets. The large, irregularly shaped pores in both coatings are partly a result of the granular areas pulling out during sample preparation. The lack of evidence of cracking in the bulk and near-surface areas of both coatings indicates that the crack sizes are very small. A probable explanation for this occurrence is the rapid cooling of the surface after deposition (Ref 2).

It may be argued that close apposition of a coating to its substrate is the first step of good mechanical bonding. Therefore, the close apposition of both coating materials to the titanium substrates could lead to good coating-to-substrate bond strengths. Other coating materials in the wear and superconducting coating fields have been shown to gain improved coating-to-substrate bond strength when applied by HVOF thermal spraying rather than plasma spraying (Ref 18-23). Some investigators have suggested that this is due to the higher impinging forces of the particles on the metal (Ref 20, 24). Other data indicate that these higher impinging forces create a denser microstructure than that produced by plasma spraying (Ref 19-22).

6. Conclusion

In this study, the HVOF thermal spraying process was used to produce HA and FA coatings on titanium substrates. The coatings exhibited good contiguity over the substrate, with good apposition. Analyses of the powders and the coatings by FTIR and XRD indicate that the coatings are very similar to the starting powders in terms of chemistry and microstructure. As a result, HVOF thermal spraying appears to be capable of producing apatitic coatings that completely cover the substrate, with little cracking or porosity. However, before the process can be recommended for commercial use, it requires further optimization by relating coating apposition to bond strength and by minimizing phases other than HA or FA.

References

1. H.W. Denissen, W. Kalk, A.A.H. Veldhius, and A. van der Hoof, Eleven Years of Study of Hydroxyapatite Implants, *J. Prosthet. Dent.*, Vol 61 (No. 6), 1989, p 706-712
2. K. de Groot, C.P.A.T. Klein, J.G.C. Wolke, and J.M.A. de Blieck-Hogervorst, Plasma-Sprayed Coatings of Calcium Phosphate, *CRC Handbook of Bioactive Ceramics: Volume II, Calcium Phosphate and Hydroxylapatite Ceramics*, T. Yamamuro, L.L. Hench, and J. Wilson, Ed., CRC Press, 1990, p 133-142
3. K.A. Thomas, S.D. Cook, R.J. Haddad, J.F. Kay, and M. Jarcho, Biological Response to Hydroxylapatite-Coated Titanium Hips: A Preliminary Study in Dogs, *J. Arthroplasty*, Vol 4 (No. 1), 1989, p 43-53
4. M.T. Manley and R. Koch, Clinical Results with the Hydroxyapatite-Coated Omnifit Hip Stem, *Dent. Clin. North Am.*, Vol 36 (No. 1), 1992, p 257-262
5. K. de Groot, Hydroxylapatite Coatings for Implants in Surgery, *Ceramics in Clinical Applications*, P. Vincenzini, Ed., Elsevier Science, 1987, p 381-386
6. P. Ducheyne, S. Radin, M. Heughebaert, and J.C. Heughebaert, Calcium Phosphate Ceramic Coatings on Porous Titanium: Effect of Structure and Composition on Electrophoretic Deposition, Vacuum Sintering and In Vitro Dissolution, *Biomaterials*, Vol 11 (No. 4), 1990, p 244-254
7. P. Ducheyne, W. Van Raemdonck, J.C. Heughebaert, and M. Heughebaert, Structural Analysis of Hydroxyapatite Coatings on Titanium, *Biomaterials*, Vol 7, 1986, p 97-103
8. E. Lugscheider, T.F. Weber, and M. Knepper, Production of Biocompatible Coatings of Hydroxyapatite and Fluorapatite, *Thermal Spray Technology—New Ideas and Processes*, D.L. Houck, Ed., ASM International, 1989, p 337-343
9. K.A. Gross and C.C. Berndt, Thermal Spraying of Hydroxyapatite for Bioceramic Applications, *Key Eng. Mater.*, Vol 124, 1991, p 53-55
10. K. de Groot, R. Geesink, C.P.A.T. Klein, and P. Serekian, Plasma Sprayed Coatings of Hydroxyapatite, *J. Biomed. Mater. Res.*, Vol 21, 1987, p 1375-1381
11. S.D. Cook, K.A. Thomas, J.F. Kay, and M. Jarcho, Hydroxyapatite-Coated Titanium for Orthopedic Implant Applications, *Clin. Orthop. Rel. Res.*, Vol 232, 1988, p 225-243
12. R.Z. LeGeros, *Calcium Phosphates in Oral Biology and Medicine*, Karger, 1991
13. K. de Groot, C.P.A.T. Klein, J.G.C. Wolke, and J.M.A. de Blieck-Hogervorst, Chemistry of Calcium Phosphate Bioceramics, *CRC Handbook of Bioactive Ceramics*, T. Yamamuro, L.L. Hench, and J. Wilson, Ed., CRC Press, 1990, p 3-15

14. L.L Hench, Bioceramics: From Concept to Clinic, *J. Am. Ceram. Soc.*, Vol 74, 1991, p 1487-1510
15. R.Y Whitehead, The Effect of Dissolution on Plasma Sprayed Hydroxylapatite Coatings on Titanium, *Clin. Mater.*, Vol 12, 1993, p 31-39
16 J.G.C. Wolke, K. de Groot, T.G. Kraak, W. Herlaar, and J.M.A. de Blieck-Hogervorst, The Characterization of Hydroxylapatite Coatings Sprayed with VPS, APS, and DJ Systems, *Thermal Spray Coatings: Properties, Processes and Applications*, T.F. Bernecki, Ed., ASM International, 1992, p 481-490
17. J.G.C. Wolke, W.J.A. Dhert, C.P.A.T. Klein, J.M.A. de Blieck-Hogervorst, and K. de Groot, The Characterization of Plasma-Sprayed Fluorapatite Coatings for Biomedical Applications, *Ceramics in Substitutive and Reconstructive Surgery*, P. Vincenzini, Ed., Elsevier, 1991, p 285-294
18. C.C. Berndt and K.A. Gross, Characteristics of Hydroxylapatite Bio-Coatings, *Thermal Spray: International Advances in Coatings Technology*, C.C. Berndt, Ed., ASM International, 1992, p 465-470
19. D.W. Parker and G.L. Kutner, HVOF-Spray Technology: Poised for Growth, *Adv. Mater. Process.*, Vol 139 (No. 4), 1991, p 68-74
20. N. Wagner, K.Gnädig, H. Kreye, and H. Kronewetter, Particle Velocity in Hypersonic Flame Spraying of WC-Co, *Surf. Technol*, Vol 22, 1984, p 359-368
21. P. McGinn, M. Jain, V. Anand, and D. Lee, Thermally Sprayed Coatings of $YBa_2Cu_3O_{6+x}$, *Thin Solid Films.*, Vol 166, 1992, p 163-170
22. P. McGinn, M. Jain, and D. Lee, Coatings of $YBa_2Cu_3O_{6+x}$ Thermal Sprayed Using the Jet Kote™ Process, *Surf. Technol.*, 1989, p 359-368
23. J.P. Kirkland, R.A. Neiser, H. Herman, et al., Thermal Spraying Superconducting Oxide Coatings, *Adv. Ceram. Mater.*, Vol 2 (No. 3b), 1987, p 401-410
24. M.L. Thorpe and H.J. Richter, A Pragmatic Analysis and Comparison of the HVOF Process, *Thermal Spray: International Advances in Coatings Technology, C.C. Bendt, Ed., ASM International, 1992, p 137-147*